Tunnelling and Underground Space Technology 162 (2025) 106603

Contents lists available at ScienceDirect

Tunnelling and Underground Space Technology incorporating Trenchless Technology Research

journal homepage: www.elsevier.com/locate/tust

Performance of the corrugated metal pipe sliplining method using FRP pipes

Aluth Premasuriya, Weena Lokuge *, Warna Karunasena, Allan C. Manalo

School of Engineering, Centre for Future Materials (CFM), University of Southern Queensland, Toowoomba, Queensland 4350, Australia

ARTICLE INFO

Keywords:
Corrugated Metal Pipes
Rehabilitation
Sliplining
FRP
Hashin Damage
CLSM

ABSTRACT

Corrugated Metal Pipes (CMP) have been extensively used in culverts for decades. Currently, there is a significant growing demand for CMPs to be either replaced or rehabilitated due to their deterioration caused by corrosion. Sliplining is one of the simplest and cost-effective methods of CMP culvert rehabilitation. This paper examined the structural performance of CMP sliplined by Fibre Reinforced Polymer (FRP) composites considering the effects of host pipe and the grout infill. In this research, CMP, FRP pipe and FRP sliplined CMP were subjected to parallel plate load test (PPLT) and the load deflection behaviour and failure modes were examined. A low strength flowable mortar mix was used as the Controlled Low Strength Material (CLSM) to fill the annular space between pipes. It was observed that the core failure of the FRP pipe governs the failure of the sliplined CMP. A change in load deflection behaviour of the host pipe of sliplined CMP system was also observed with reference to the PPLT results of the FRP pipe sample itself. Further, the failure modes of the FEM and the failure modes observed in the experiments were in good agreement.

1. Introduction

The use of Corrugated Metal Pipes (CMP) for culverts seems extensive in most parts of the world being a low-capital option (Gonilha et al., 2022; Heywood and Pritchard 2011; Highways England, 2020). Light weight and less turnaround time for design and installation are other advantages of CMP. However, the major drawback of CMPs is their deterioration caused by corrosion, which could result in unsafe infrastructure for road users and the community. This rate of deterioration of corrugated metal structures due to corrosion was higher than expected (Gonilha et al., 2022). In some instances, metal culverts have corroded within three years of installation due to the contaminants in the backfill soil and the potential aggressive nature of the water flowing through the soil covering the culvert (Taha and Halter, 2019). Another reason for the growing demand for metal culverts to be replaced or rehabilitated is the fact that culverts (similar to all other road infrastructure) are being exposed to increasing traffic loads than they were originally designed for (Heywood and Pritchard 2011). Legal load limits of road infrastructures were increased compared to the limit adopted in the bridge design loadings in late 1970 s (Gordon and Boully, 1998). Adopting mass limits on road structures to suit the original design loads, limits the productivity of the road transport system (Heywood and Ellis 1998).

Although corrosion of corrugated metal pipes in culverts is unavoidable (Heywood and Pritchard 2011; Kunecki et al., 2016), it will continue to be an economical option for rural roads. Hence understanding the behaviour of the corroded culvert is important in the process of its rehabilitation to effectively restore its structural integrity towards the resilience of rural community. The most vulnerable area for a metal pipe culvert is usually the invert (García and Moore, 2015). A number of studies found that the corrosion of the CMP negatively affects structural stability of the culvert (El-Taher and Moore, 2008; Kunecki et al., 2016). For instance, El-Taher & Moore (2008) revealed that the reduction of the wall thickness of the pipe invert is directly proportional to the reduction in safety factor against yield. Kunecki et al. (2016) observed that the internal stress distribution in a 1400 mm diameter CMP is changed due to the material loss at the invert. Another finding of this research is that the bending moment of the pipe wall has a decisive effect on normal stress in the cross sections of the shell. This means that local pipe wall bending moments also influence the overall pipe stability. Mai et al. (2014) examined the culvert pipe response to the surface live load applied as a line load by testing two deteriorated pipe samples of 1800 mm diameter and observed a non-linear load–deflection behaviour. Additionally, Mai et al. (2014) noted that the 2-D Abaqus model was unable to represent the real behaviour of the samples due to

* Corresponding author.
E-mail address: weena.lokuge@unisq.edu.au (W. Lokuge).

https://doi.org/10.1016/j.tust.2025.106603
Received 4 September 2024; Received in revised form 28 February 2025; Accepted 27 March 2025

the results being conservative. A recent experimental and numerical study demonstrates that stress concentration in the circumferential direction are greater than those in the longitudinal direction for a buried corroded pipe (Zhang and Wong, 2023).

The conditions of deteriorated CMP culverts are generally assessed by visual inspections that provide only qualitative data about corrosion levels (Department of Transport and Main Roads QLD, 2015; Highways England, 2020; Regier et al., 2018). Regier et al. (2018) has attempted to quantify the extent of corrosion of the pipe invert to determine the end-of- service life condition based on its remaining strength. Six samples with different levels of corrosions at the pipe invert were tested. However, it was unable to quantify the critical corrosion in this experimental study and found that corrosion was only one of the various factors (example: elastic modulus of backfill soil and burial depth of pipe) affecting the culvert behaviour. Further, Regier et al. (2018) concluded that soil stiffness of the backfill had a greater impact on the overall behaviour than the level of steel corrosion of the CMP. This is because the critical level of corrosion may dictate the failure mechanism leading to local buckling of the pipe wall between perforations. On the other hand, García & Moore (2015) observed that perforations due to the corrosion reduces the structural capacity of the culvert and may generate erosion of the soil through the holes which will further reduce the capacity of the soil-pipe structure. In recent studies, in addition to the traditional qualitative assessments mentioned earlier, field tests, strain measurements, and deflection measurements using Digital Image Correlation (DIC) techniques were also used to evaluate the extent of deterioration (Safari et al., 2023). Furthermore, Safari (2023) noted that the maximum and minimum values of the Dynamic Amplification Factor are correlated to the local effects of corrosion and damage to the culvert.

In response to CMP deterioration challenge, several culvert rehabilitation techniques are used all over the world. The remove and replace method is a conventional method of rehabilitation which requires traffic diversion whereas trenchless options such as concrete invert, concrete in-situ lining, sliplining, spiral wound plastic structural lining, pipe jacking and pipe bursting enable retrofitting the culvert with minimum disruption to the road users. However, sliplining is one of the increasingly used rehabilitation methods (Rahmaninezhad et al., 2019). Many different types of materials, such as high-density polyethylene (HDPE), polyethylene, polypropylene, polyvinyl chloride (PVC) and fibre-reinforced polymer (FRP) composites, are commonly used in the sliplining of CMP culverts (Minnesota Department of Transport, 2016). Several studies on sliplining rehabilitation have focused on HDPE and PVC linings (Rahmaninezhad et al., 2020; Rahmaninezhad et al., 2019; Tetreault et al., 2020). However, the durability of the HDPE and strength of the PVC have been questioned in the literature (Taha and Halter, 2019). While their initial costs may be lower, life cycle costs could be higher because of durability issues. FRP pipe sliplining is one of the accepted methods by the pipeline infrastructure committee of the American Society of Civil Engineers (Osborn, 2009). In addition to CMP rehabilitation, this method is used to rehabilitate prestressed concrete pipes too (Zhu et al., 2021). Corrosion resistance, lower transport and production cost, ease of repairs or maintenance and high durability against unfavourable weather conditions are also significant advantages of FRP composite pipes (Ehsani 2019; Prabhakar et al., 2019).

Eshani (2019) suggested that the sliplining repair method using sandwich FRP composite pipes is an efficient alternative to metal pipe culvert rehabilitation. The weight of this FRP composite pipe is as low as 10 %-15 % of the weight of conventional solid wall fibreglass pipes and is significantly lighter than steel or concrete pipes. Lightweight is a key attribute of FRP sliplining compared to the conventional sliplining techniques with concrete pipes. It contributes to the ease of installation greatly by eliminating the need for heavy machinery. However, only a few studies have been carried out to investigate the structural behaviour of FRP sliplining method (Abdellatef et al., 2021; Ehsani 2019; Hudson et al., 2023; Kanagaraj 2020; Park et al., 2014; Zhao et al., 2004). Most of these experimental and numerical studies on FRP pipes are limited to parallel plate loading without having the host pipe and grout infill which may not be the real representation of the sliplined pipe as the flexibility of the pipe system may be affected by the grout and host pipe. Other than that, it is important to study whether the effect of the remaining portion of the metal pipe is beneficial or not to the sliplined pipe system. The remaining strength of the host pipe could be beneficial if the sliplined pipe system is stronger than the FRP pipe alone due to the composite action. On the other hand, it is important to investigate whether the CMP and grout infill could generate high-stress concentration areas on the FRP pipe surface, leading to a local bending failure on the pipe wall. Even though numerical study of Abdellaief (2021) comprises a FE model with CMP and FRP, the corrugated pipe was approximated to a cylinder although the behaviour of a cylindrical pipe and a flexible corrugated pipe may not be the same.

Modified Lowa formula has been widely used in buried flexible pipe design (Masada 2000). In contrast, Hudson (2023) observed that the deflection assessment of buried CMP using multi-physics simulation is in better agreement with full-scale tested CMP compared to the analytical evaluation using the modified Lowa formula. A numerical study shows that the vertical eccentricity of the carrier pipe of a sliplined pipe system leads to increased stresses in both the carrier pipe and the host pipe. (Zhao et al., 2004).There are well established design standards available for the buried flexible pipe design (Standards Australia, 1998, 2011). Since no specific design standard is available for the design of sliplined pipe systems, buried flexible pipe system standards are being used to design a sliplined pipe culvert. In the prevailing FRP slipline design practice, loads are applied assuming a uniformly distributed pressure on the pipe surface radially and neglects any contribution from the remaining CMP section and grout. The validity of the load distribution assumption has not been verified in the past literature related to FRP sliplining whereas neglecting the remaining strength of CMP may lead to a conservative design. This research paper focusses on the effects of host pipe and the grout infill on the performance of the sliplined pipe system. The numerical investigation will enable to predict the performance of sliplined pipe systems of different diameters without carrying out load tests which is a costly experience.

This research examined the performance of CMP with a FRP sliplining subjected to parallel plate load test. It experimentally evaluated the load deflection and failure modes of the sliplined pipe system. Controlled Low Strength Material (3 MPa flowable mortar) was used to fill the annular space between the CMP and the FRP structural lining in the pipe sample preparation. In addition to the sliplined pipe sample CMP and FRP pipes were also tested as control samples. The study also includes a finite element analysis to predict the load–deflection relationship, strain responses, and failure modes. The results of this study will provide practicing engineers and researchers with sufficient information about the performance of the CMP retrofitted with FRP sliplining, leading to opt for this method resulting in significant time savings for the rehabilitation of corrugated metal pipe culverts.

2. Material characterization

Damaged host pipe, new carrier pipe and the infill material between new and the host pipe are identified as the three main parts of a sliplined pipe system. A sandwich FRP composite pipe was used as the new carrier pipe and a flowable mortar used as the infill material in this study. Both composite materials and infill materials were characterised while CMP materials properties were based on the available literature.

2.1. FRP Composite Materials

StifPipe®, the pipe used to retrofit the corrugated metal pipe comprises four layers of composite material (Fig. 1). The first layer (i.e., innermost layer) and fourth layer are identical and made of 1.02 mm thick Glass Fibre Reinforced Polymer (GFRP) composites. The second layer is a 1.7 mm thick Carbon Fibre-Reinforced Polymer (CFRP)

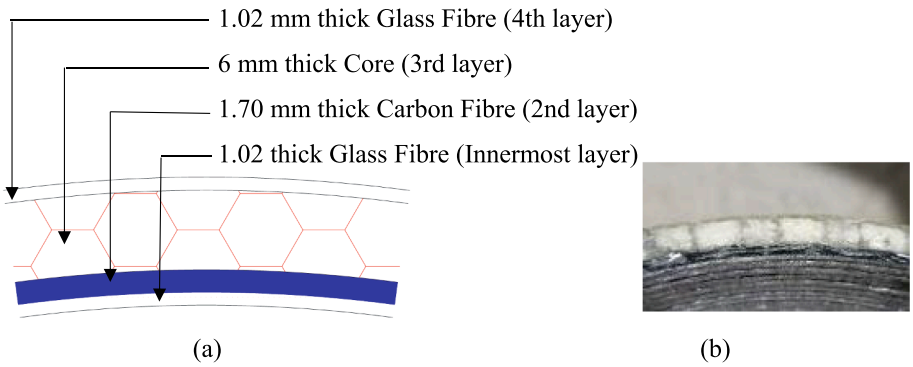

Fig. 1. (a) Cross section; (b) Close up image of StifPipe wall.

composites. Both CFRP and GFRP layers are fabricated by saturating carbon fire and glass fibre fabrics in epoxy resins respectively. A 6 mm thick core, lightweight honeycomb layer is sandwiched between the second and fourth layers. GFRP lamina comprises bidirectional glass fibres which are present in both circumferential (0^0) and longitudinal (90^0) directions of the pipe whereas CFRP lamina is unidirectional, and fibres are oriented and distributed only along circumferential direction. In this testing program, GFRP and CFRP lamina were characterised in each direction as individual laminas using tensile, compression and shear tests. Further, the laminate was also characterised to determine the effective properties of each direction using the same test method.

2.1.1. FRP material testing program

Tensile testing was carried out on FRP samples following ISO 527–4 (International Organization for Standardization, 2021) standard to establish the mechanical properties including peak strength, modulus of elasticity. Ten samples per each structural layer of pipe were cut from a large FRP sheet using a waterjet-cutting technique (Fig. 2(a)). Type 1B specimens (also known as dog bone specimens) were used in these experiments. Further five more dog bone samples were tested for 11.2 mm thick laminate to determine the effective tensile properties (Fig. 2(b)). The test was conducted using an MTS Universal Testing Machine (UTM) with a capacity of 100 kN at a loading rate of 2 mm/min and the load was applied up to failure as per ISO 527–4 (International Organization for Standardization, 2021). Further, minimum of two coupons were instrumented with a 5 mm uniaxial strain gauge (FLAB-5–11-1LJC-F) bonded longitudinally in the middle of the coupon to determine the strain behaviour. The data of the load–displacement curves was obtained from the testing machine while a data logger system was used to get the strain values from the gauges at a rate of 10 readings per second.

Compression test was conducted in accordance with ASTM D6641standard to determine the compressive strength of each FRP layers. Ten samples per each structural layer of pipe were cut from the same FRP sheets mentioned above to represent both 0^0 and 90^0 directions (Fig. 3(a)). Compression test was carried out using the same UTM attached with the combined loading compression test fixture at a load of 1.3 mm/min and the load was applied up to failure as per ASTM D6641(ASTM International, 2016a). Finally, the shear test was conducted following V-notched beam method in accordance with ASTM D5379. All shear test coupons were instrumented with a 3 mm uniaxial strain gauge (FLAB-3–11-3LJC-F) bonded longitudinally in the middle of the coupon. Shear test coupons are shown in Fig. 3(b). UTM with V-notch beam test fixture was operated at a loading rate of 2 mm/min and the load was applied up to failure as per ASTM D5379 (ASTM International, 2019). Test standards and coupon sample sizes used in this testing program is summarised in Table1.

2.1.2. FRP material testing results

The tensile load–displacement curves of the tested coupons are shown in Figs. 4 & 5. Generally, the load–displacement responses of all coupons exhibited a linear behaviour up to the peak load except the 0^0 direction CFRP coupons which showed a gradient reduction before its failure. Further a sudden load drop at the failure load was common to all load displacement curves. The average failure loads were determined to be 230 MPa and 139 MPa for GF coupons in circumferential and transverse directions, respectively. A significant difference was observed in the failure loads in each direction for CFRP coupons. The average failure loads of 0^0 direction CF coupons were 960 MPa whereas the average failure load of 90^0 direction samples was as low as 7 MPa. Elastic modulus and failure stress of each lamina and the laminate were calculated by plotting the stress against the stain and results are tabulated in Table 2. The tensile failure occurred within the gauge length with no signs of end slips (Fig. 6).

Compressive strengths of each structural layer and the FRP laminate was determined based on the peak load. CFRP specimens and FRP laminate specimens failed in compression whereas GFRP specimens reached its peak load due to buckling invalidating the experiments (Fig. 7(a)). Therefore, the compressive strength of the GFRP lamina was estimated based on the ratio between compressive and tensile strengths by comparing the same ratio of similar material from the available

Fig. 2. (a) Tesile specimens of layer 1 & 2; (b) Tesile specimens of laminate.

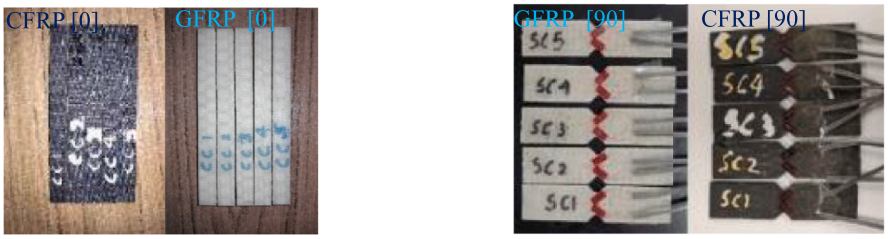

Fig. 3. (a) Compression test specimens; (b) Shear test specimens.

Table 1
FRP characterization details.

Test	Test standard	Dimension (mm) Length	width
Tensile (0^0 and 90^0)	ISO 527–4	200	20
Compression (0^0 & 90^0)	ASTM D6641	140	13
Shear	ASTM D5379	76	19

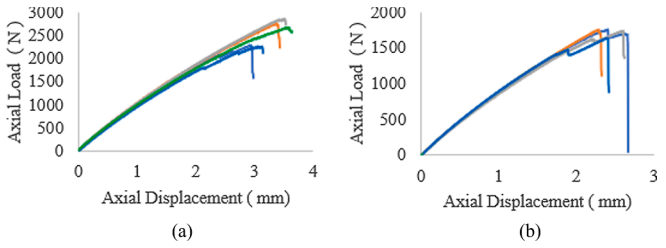

Fig. 4. (a) GFRP [0^0] load deflection curves; (b) GFRP [90^0] load deflection curves.

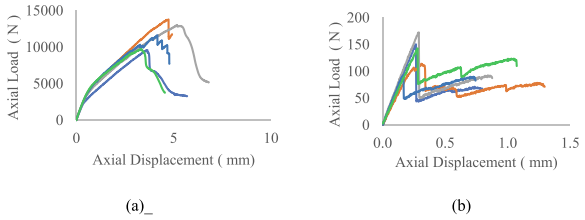

Fig. 5. (a) CFRP [0^0] load deflection curves; (b) CFRP [90^0] load deflection curves.

literature (Al-saadi et al., 2019; Otoom et al., 2022). 60 % of tensile strength is assumed as the compressive strength of the GFRP lamina for the FEM. Shear strength and shear modulus of each structural layer was determined by plotting shear load displacement curve and shear stress strain curve respectively. The shear failure occurred along the notch by the formation of vertical shear cracks (Fig. 7(b)). Compressive and shear properties are also tabulated in Table 2.

2.2. Infill Materials

Infill material between the host pipe and the new carrier pipe of a sliplined pipe system also plays an important role in facilitating load transfer between pipes. Tetreault et al. (2020) observed a rigid pipe behaviour when a field test was carried out for a CMP sliplined using HDPE pipe and high-density grout in contrast to the flexible behaviour observation when the same test was conducted using low-strength grout. Therefore, a low-strength cementitious grout, CLSM was used in the

Table 2
FRP tensile, compressive and shear test results.

Property	Material	Orientation θ^0	Value (COV[a])(%)
Elastic modulus, GPa	GFRP	0	16.75 (16.1)
	GFRP	90	11.88 (13.9)
	CFRP	0	85.93 (7.8)
	CFRP	90	3.35 (11.8)
	LAMINATE	0	7.09 (6.6)
	LAMINATE	90	2.97 (16.1)
Tensile strength, MPa	GFRP	0	230 (10.0)
	GFRP	90	139 (6.0)
	CFRP	0	690 (16.5)
	CFRP	90	7 (23.2)
Compressive strength, MPa	CFRP	0	128 (19.1)
	CFRP	90	20 (26.2)
Shear modulus, GPa	GFRP	90	0.22 (10.2)
	CFRP	90	1.00 (19.5)
Shear strength, MPa	GFRP	90	126 (10.0)
	CFRP	90	47 (14.6)

[a] Coefficient of Variation:

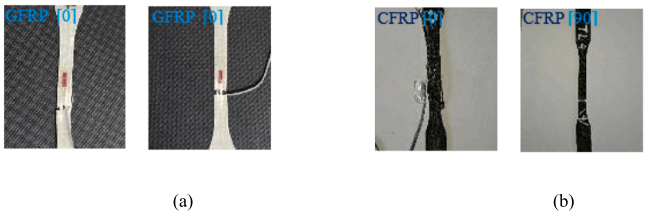

Fig. 6. (a) Failed GFRP tensile specimens; (b) Failed CFRP tensile specimens.

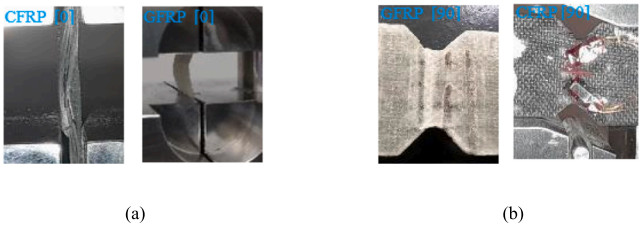

Fig. 7. (a) Failed compression specimens; (b) Failed shear specimens.

experimental and numerical studies in this paper since high-strength grout was found by previous researchers to decrease the sliplined pipe system flexibility.

2.2.1. Grout testing program

The CLSM was achieved by mixing GP cement, fly ash, and granular material in a ratio of 6:2.5:78 by mass, following the guidance in Appendix K of the AS/NZS 2566.2 – Australian Standards for Buried Pipelines – Installation (Standards Australia, 2022). Table K2 of the

same standard was followed when selecting the granular material. Mass passing percentage of 19 mm and 0.075 mm sieve was 100 % and 20 %, respectively. Commercially available CLSM grout was used to fill the annular space of the test samples. In preparation of CLSM grout cementitious and granular material mix well in a rotating drum and water as added afterward. Six cylinders were cast with CLSM grout using 100 mm diameter by 200 mm high moulds. After curing for four days in a water bath, the cylinders were stored in the laboratory at room temperature for another 24 days. Three samples were tested for compressive strength in accordance with ASTM D4832 (ASTM International, 2016b). Other three samples were used for the split tensile test to determine the tensile following ASTM C496 standard (ASTM International, 2017). A tested compression test sample and a tested tensile test sample are shown in Fig. 8(a). Both compression and tensile tests were conducted using an MTS Universal Testing Machine with a capacity of 100 kN at a loading rate of 2 mm/min and the load was applied up to failure. The maximum applied loads indicated by the testing machine at failure for each test were recorded. According to the tensile test standard the load needs to be applied at a constant rate such that the cylinder will fail in not less than 2 min. All the test samples took more than 2 min to reached to its failure load satisfying the standards.

2.2.2. Grout testing results

The load–displacement responses of all cylinders exhibited an approximate linear behaviour up to the peak load (Fig. 8(b)). All the samples failed in similar manner crushing the bottom third portion of the cylinder. The compressive stress was calculated dividing the failure load by the cross-sectional area of the cylinder. The average failure stress was 3 MPa. Split tensile strength was calculated using maximum applied load indicated by the testing machine. All the samples were failed by splitting the sample into two parts. Tensile stress was calculated following section 9 of ASTM C496 (ASTM International, 2017). Average tensile failure stress of CLSM cylinders was 0.38 MPa Results are tabulated in Table 3.

Table 3
CLSM grout test results.

Property	Average COV(%)[a]
Compressive strength of grout, MPa	3.0 (12.7)
Elastic modulus of grout, MPa	439 (4.2)
Tensile Strength of grout, MPa	0.4 (16.4)

[a] Coefficient of Variation

3. Full scale pipe testing program

Full-scale testing was conducted in two stages. FRP pipe sample alone and CMP pipe alone were tested as control samples to compare with the strength gain of the sliplined pipe due to the structural lining in stage I. In stage II, CMP samples were sliplined with FRP pipes. In both stages, samples were subjected to PPLT in accordance with ASTM D2412 (ASTM International, 2021). 300 mm x 250 mm x 20 mm thick steel plates were fabricated to use them as top and bottom plates in testing machine following ASTM2021. These plates can only fit in the 1000 kN UTS available in UniSQ test facility. While expected failure loads in this test series are range of 15 kN to 60 kN, other instrumentations used such as the DIC and the attached strain gauges verified that this level of failure load is accurate. Further, 1000kN UTS calibration report confirmed the reliability of a low measurement of 20 kN with an error of only 0.5 % and a 95 % confidence interval of +/- 0.8 % of the measured force. The test set up is shown in Fig. 9.

Each test was continued until the failure of the specimen and load–deflection relationship was recorded. Further, Digital Image Correlation using Video Guage V.5.4.4 software was used to record the vertical and horizontal diameter change of the host pipe due to loading. The accuracy of the DIC measurements is 10 μm based on the actual width of the area viewed in image. The video of the DIC system was also used to examine the failure mode of the FRP pipe and the location of the failure.

3.1. Pipe testing program

In stage I, both carrier pipe and host pipes were tested itemise. First, 300 mm long two FRP pipe samples were tested. Pipe wall thickness was measured in three locations of the pipe diameter and average thickness was 11.2 mm. Average internal diameter of the FRP pipe was 215 mm whereas external diameter was 236 mm. As the FRP pipe wall is whitish in colour, the pattern of speckles was applied to the pipe wall using a black permanent marker to increase the measurement resolution of the DIC system. The strain measurement method of the video gauge software was used to measure the diameter change. Firstly, two virtual strain gauges were positioned at the midpoints of the pipe wall in the horizontal diameter of the pipe. Having physically measured the distance between strain gauges to the nearest millimetre using a steel ruler, the actual diameter of the pipe was input to the DIC software enabling the software to produce output as a length rather than a strain. The same procedure was adopted to measure the vertical diameter change. The UTM was operated at a displacement rate of 12.5 mm/min following ASTM D2412. Two samples of CMP having 305 mm external diameter was also tested as same manner. Same sample length and the same displacement rate were maintained in the experiment. The thickness of the CMP was 1.6 mm whereas lock seam was four times thicker than the other areas. The pitch and the depth of the helical sinusoidal profile was 60 mm and 13.5 mm respectively. Helix angle measured from its axis was 82.5^0. Four pieces of papers were glued to each end of vertical and horizontal diameters of the pipe sample to increase measurement resolution in DIC system.

In stage II, 300 mm long two Sliplined Corrugated Metal Pipe (SCMP) samples were tested. Strain variation of the grout was also measured

(a) (b)

Fig. 8. (a) CLSM test specimens; (b) Compressive test load–displacement curves.

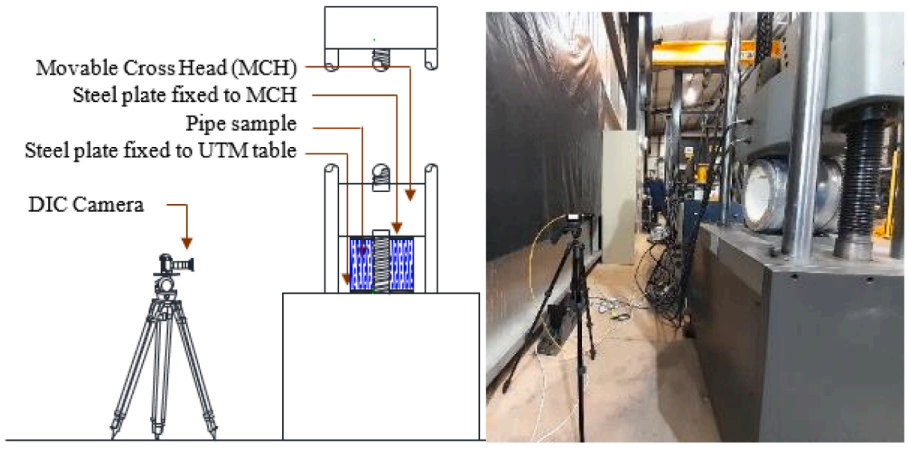

Fig. 9. (a) PPLT schematic diagram; (b) Test set up.

using strain gauges and a data logger system was used to record the readings. First, the selected locations of inside face of CMP were abrased using a sandpaper. Having cleaned the CMPs and FRP pipes thoroughly using dry clothes, 3 mm long single-element strain gauges (FLAB-3–11-3LJC-F) were fixed using cyanoacrylate adhesive in eight locations in mid-section of the pipes as shown in Fig. 10(a). The resolution of strain gauge was 1 μm/m. The exact location was 150 mm from one end in the longitudinal direction. The Resistance of the strain gauges were 120 Ω whereas strain limit in room temperature was 10,000 με.

All strain gauges were protected by providing a transparent silicon rubber coating (KE-348 T) as a waterproofing layer between grout and the sensor. Corrugated metal pipes were inserted into heavy duty polyethene bags and tied to the CMP wall with strings to close one end of the pipes to hold grout without leaking (Fig. 10(b)). 10 mm long PVC conduit pieces were tied to the outside face of the FRP pipe as spacers before placing inside the CMP to avoid excessive displacement of FRP pipe during grout pouring. To account for variations in grout thickness caused by potential buoyancy effects during construction, a spacer was chosen with a size smaller than the gap between the host pipe and the new liner., The average grout thickness was 27.5 mm and minimum and maximum thickness of the grout fill was 23 and 32 mm respectively. Two sliplined corrugated metal pipe samples were tested in parallel plate load test after 28 days of pouring of grout in the same manner as stage I.

3.2. Pipe testing results

Parallel plate load test results are discussed in two sections for clarity. Stage I results section covers the item wise load test results for CMP and FRP pipe whereas load test results for sliplined pipe is discussed in stage II results section.

3.2.1. Pipe testing results-Stage I (item wise load test for CMP and FRP pipes)

Load-deflection relationship of the FRP pipe was linear up to the pipe failure. Load- deflection curves of both samples were reasonably

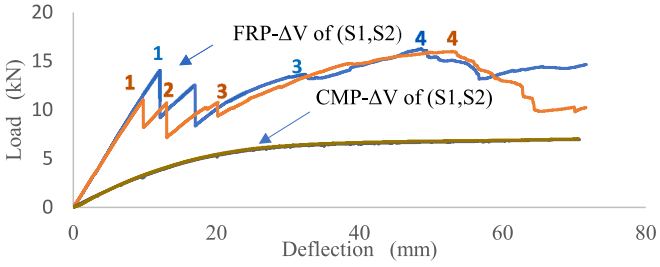

Fig. 11. Load deflection curves.

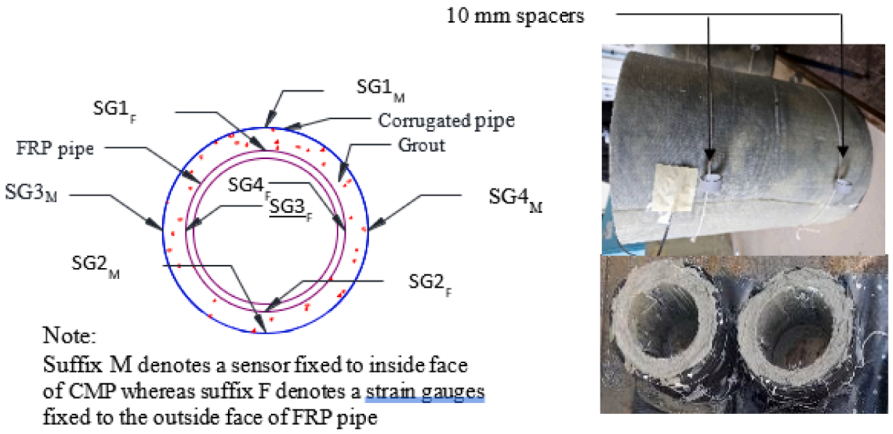

Fig. 10. (a) Sliplined pipe cross section; (b) Sliplined pipe samples.

consistent even though the failure loads are slightly different (Fig. 11). Failures of the pipes were marked as '1′, '2′,'3′, and '4′ on the load–deflection curves, where '1′ represents the first failure, with subsequent numbers indicating progressive failure stages, respectively. Both samples failed at the invert due to core failure and delamination (Fig. 13(a)) Failure loads were 13.95 kN and 10.7 kN for sample 1 and 2 respectively. Failure locations are shown by an arrow. The displacement of the movable cross head of UTM was continued even after the absolute failure (1st failure) as pipe samples exhibited more load carrying capacity. The second failure occurred at the crown and the invert simultaneously by cracking of honeycomb layer at the crown in addition to the delamination (Fig. 13(b)) while delamination at the invert further propagated. Locations of the 3rd failure were not the same for the two pipe samples. However, the damaged layer was common for both pipes. Two inner most layers of the pipe sample1 failed at the 10-clock position while the same layer of sample 2 failed at the invert (Fig. 14(a)).

The peak load of the pipe sample 1 was 16.1 kN whereas it was 15.0 kN for the pipe sample 2. The fourth failure of the sample 1 occurred at the 10–4 clock positions due to the yielding of carbon fibre layer. Further, the reversal of curvature was initiated at the invert. Similarly, the fourth failure of the sample 2 occurred at the 8–2 clock positions by yielding the carbon fibre layer. In addition to those two locations another failure was observed at the invert due to the reversal of curvature. Final failure modes are shown in Fig. 14 (b). Load deflection behaviour of two CMP samples was identical (Fig. 11). Unlike FRP samples, no significant failure was observed rather than an excessive deformation (Fig. 15). UTM load reading reached to its peak value of 7.05 kN with the ductile deformation (Fig. 10). Both horizontal (ΔH) and vertical (ΔV) diameter changes due to load for both types of pipes were plotted in Fig. 12. Diameter changes curves were plotted from zero load up to the first failure load of the FRP pipe. As diameters of FRP pipe and CMP are different, percentage diameter change was considered for the comparison. Sample 1 and 2 curves were coincided for both type of pipes.

3.2.2. *Pipe testing results – Stage II (load test for sliplined pipe as a whole)*

The load–deflection relationship is shown in Fig. 16(a), while Fig. 16 (b) displays the sample after failure. A nonlinear load deflection relationship was observed for both samples. The load deflection curves from stage I were also added for the purpose of comparison. The load deflection curves of two samples coincided until 6.5 kN load. After the sudden gradient change at 8.5 kN load, sample 2 curve gradients were slightly higher than the sample 2 until load reached 16.6 kN. '0′ marked on the load deflection curves represents sudden gradient change or minor drops prior to FRP pipe failure. The failure load of the sample 1 was recorded as 47.5 kN whereas sample 2 failed when load reached 44.0 kN. The peak load for Sample 1 was recorded at 52.7 kN, whereas Sample 2 exhibited a slightly higher peak load of 55.2 kN. '1′ and '2′ marked on the load deflection curves denotes the failure load and the peak load respectively.

Even though minor drops were present at 41.4 kN load, FRP pipes remained intact until load reached its failure loads mentioned above.

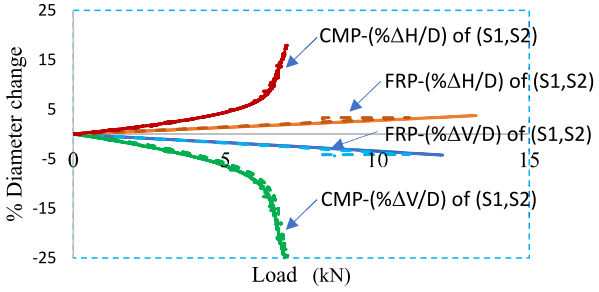

Fig. 12. Variation of diameter with applied load.

The reason for these drops and gradient change mentioned above could be due to the grout failure. This is evidenced by the strain gauge reading SG2F and SG3F (Fig. 17) which exceeds their limiting tensile strain of 1000 με. The pipe failure moments were captured by the DIC video whereas grout failures mentioned above could not be captured as they were not at the grout face. Both FRP pipes (carrier pipes) of the sliplined pipe sample failed due to core failure and delamination at the invert which is the same failure location when PPLT carried out for FRP pipes alone mentioned in section 3.2.1 (Fig. 16(b)).

4. Finite element model (FEM) simulation

FEM simulation is implemented to understand in detail the overall behaviour of FRP sliplined pipe system under different loading conditions with the aim of conducting a parametric study. This section provides details of the development of FE models to predict the load deflection behaviour and the failure mode of the sliplined pipe system. The FE models were developed using commercial software package Abaqus (Dassauts Systems, 2019).

4.1. *Model development*

FEM model was developed in three stages. The first model was to simulate the PPLT of FRP pipe alone. The characterized FRP material properties in section 2 were used in this FEM. Secondly, a model for PPLT of CMP alone was created. Finally, the sliplined pipe system model was developed using the parts created for the other two models mentioned above. In each stage FEM models were validated by the experimental results presented in section 3. Static analysis method was used in this simulation to save computational time and the memory usage of the computer. The nonlinear analysis (NLGEOM) option was also activated, allowing relatively large displacements.

4.1.1. *Material properties used in FEM*

To model the FRP pipe, all GFRP and CFRP properties listed in section 2 was utilized The first, second and fourth layers were modelled to have the FRP properties listed in Table 2 with the core (3rd layer) properties taken from the technical data sheet (Lantorcomposites.com, 2021) provided by the supplier. Table 4 shows the properties of the core of the FRP pipe. Hashin damage criterion was incorporated in this simulation to model the damage initiation of each FRP layers of pipe (Hashin, 1980). The fracture energies in FRP layers which is required for damage evolution were assumed to be 2 N/mm and 0.33 N/mm for longitudinal and transverse direction respectively (Wong et al., 2011). When modelling the CMP, the plastic model in Abaqus was used to simulate the plastic behaviour of steel. The yield strength and the ultimate strength used in the plastic model were 320 N/mm2 and 390 N/mm2 respectively (Garifullin et al., 2021). Infill layer (grout) was modelled using the CLSM properties listed in Table 3 of section 2.

4.1.2. *Model 1- FRP pipe on parallel plate load test*

The global coordinate system of the model was defined as the positive Z-axis was parallel to the longitudinal axis of the cylinder. One of the edge points of the pipe crown was selected as the origin (Fig. 18(a)). The FRP pipe was modeled as shell elements with composite layup whereas steel bottom plates and loading plates were created as solid homogeneous elements. Each layer of composite layup was created as elastic lamina with sub-options of hashing damage, damage evolution and damage stabilization. After completing all the required parameters in both longitudinal and transverse directions in edit material dialog box, the correct orientation of composite layup was achieved by defining a datum cylindrical coordinate system.

Boundary conditions were applied to the steel plates in the initial step to accurately reflect the movements of the testing machine components. The bottom plate was assumed restrained for all rotational and translational degrees of freedom. The loading plate was restrained to all

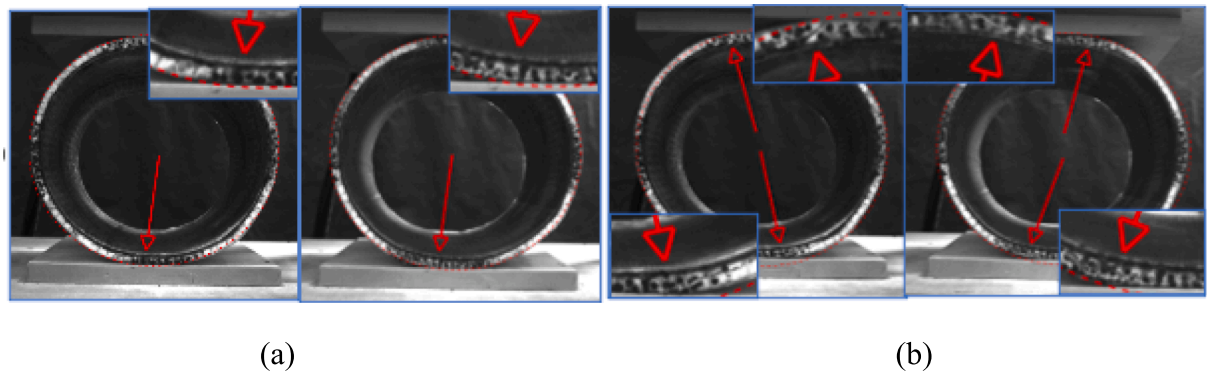

Fig. 13. (a) 1st failure of FRP pipe samples; (b) 2nd failure of FRP pipe samples.

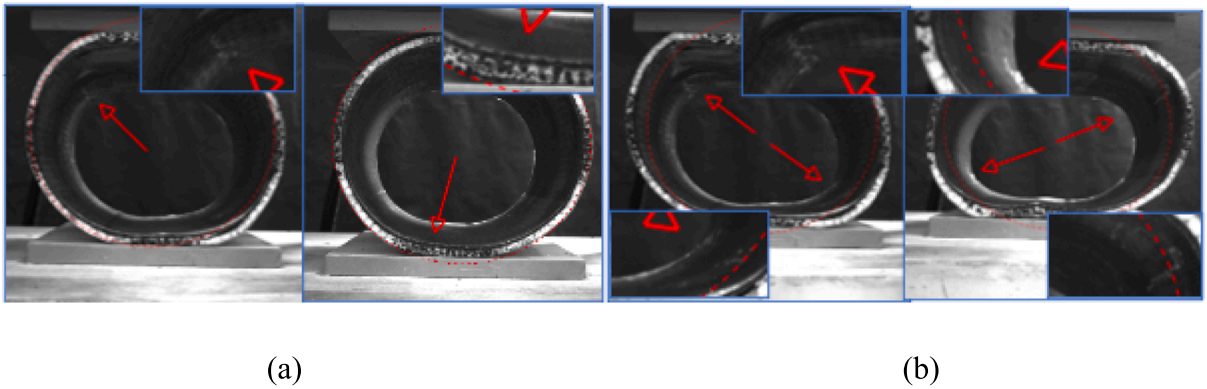

Fig. 14. (a) 3rd failure of FRP pipe samples; (b) 4th failure of FRP pipe samples.

Fig. 15. (a) CMP sample before testing; (b) CMP sample after testing.

degrees of freedom except Y direction translational freedom enabling movements in the Y direction under concentric displacement control. In the experiment pipes are held in position between plates only by the normal and frictional forces. Two steps were created to mimic the same testing procedure. Initially, steel plates and pipes are unconnected. Contact between unconnected parts, namely loading plate, bottom plate and pipe were achieved in the contact step (1st step) by providing a negligible downward movement to pipe and top plate. In the loading step (2nd step), 25 mm downward displacement was applied as the displacement control simulation was carried out. All the parts are held in position during the loading step due to the defined frictional interaction property and the frictional coefficient was assumed to be 0.1. Both experimental and FEM Load deflection curves were plotted in Fig. 20(a). Damaged layers that satisfied the Hashin damage criteria were also examined. FEM captured both 1st and 2nd failure similar to sample 1.

4.1.3. Model 2- CMP on parallel plate load test

The second FEM was created to simulate the PPLT of CMP alone. The second model used the same boundary conditions, steps, contact method, and loading as the first model, but with different pipe geometry and properties. The CMP was created as a homogeneous shell element, along with a solid spiral to simulate the lock seam area of the pipe (Fig. 18(b)). The solid part and the shell part of the pipe were connected using shell-to-solid coupling constraints. Load deflection curves from the experiment and FEM were plotted together for comparison (Fig. 20(b)).

4.1.4. Model 3- sliplined CMP on parallel plate load test

Finally, the sliplined pipe model was created using the second model

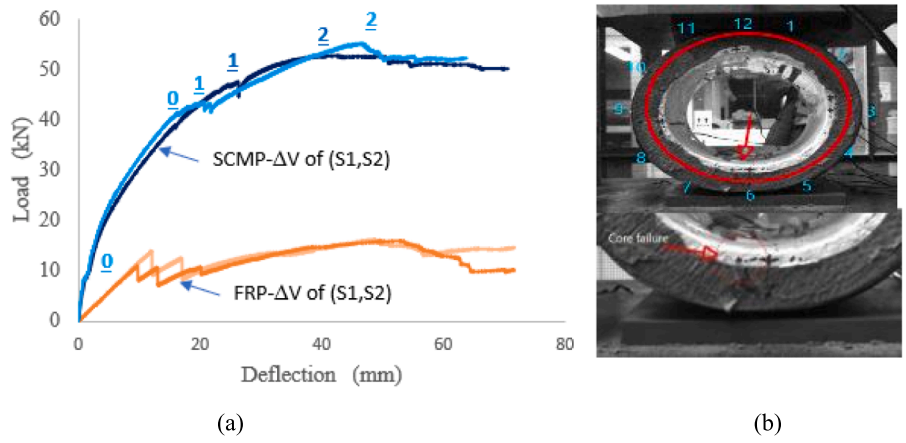

Fig. 16. (a) Load deflection curves; (b) Failed sliplined pipe sample.

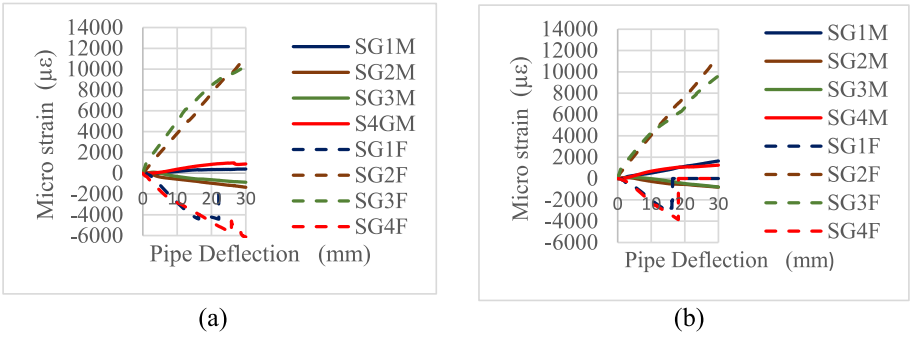

Fig. 17. Strain guage reading for (a) sample 1; (b) sample 2.

Table 4
Material properties of the core of the FRP pipe (from manufacturer).

Property	Value
Elastic Modulus, MPa	800
Tensile Strength, MPa	4
Compressive Strength, MPa	8
Shear Modulus, MPa	35
Shear Strength, MPa	3.5

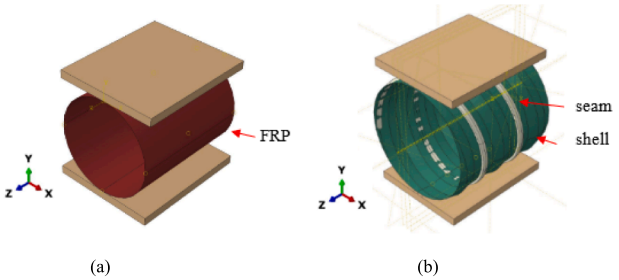

Fig. 18. (a) FE Model 1 for FRP pipe; (b) FE Model 2 for CMP pipe.

and the FRP pipe from the first model (Fig. 19). The CLSM grout layer between the CMP and FRP pipe was created as a 3D deformable part. Due to the complexity of the shape two parts were created. These two parts were combined using tie constraints instead of merging into a single part as the merged part led to convergence issues due to the complexities in the mesh. 10-node quadratic tetrahedron element type

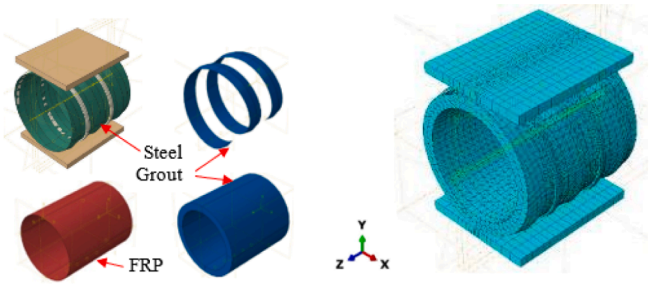

Fig. 19. (a) Parts of FE Model 3; (b) FE Model 3 for SCMP.

(C3D10) mesh was assigned to the solid parts mentioned above. CMP, CLSM grout layer and FRP pipe were connected to each other by tie constraints.

In this study, the Concrete Damaged Plasticity (CDP) model in Abaqus was used to simulate the plastic behavior of CLSM grout. The CDP model considers compressive crushing and tensile cracking as the two main failure mechanisms. Fig. 21 (a) shows the response of CLSM grout to uniaxial loading plotted based on experimental results in section 3, along with the main plasticity parameters of the simplified concrete damage plasticity model (Hafezolghorani et al., 2018). A dilation angle of 31^0 was assumed while eccentricity and invariant stress ratio (K) values were assumed to be 0.1 and 0.67, respectively. The ratio of initial biaxial compressive yield stress to initial uniaxial compressive yield stress was 1.16. To reduce computational time, a viscosity parameter value of 0.0005 was used instead of the default value of zero

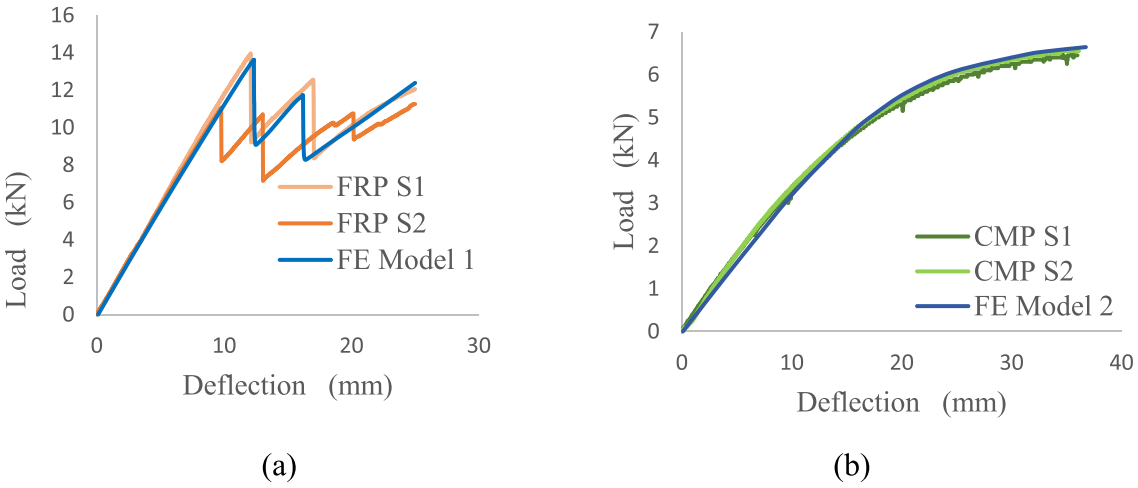

Fig. 20. (a) Validation of FEM 1; (b) Validation of FEM 2.

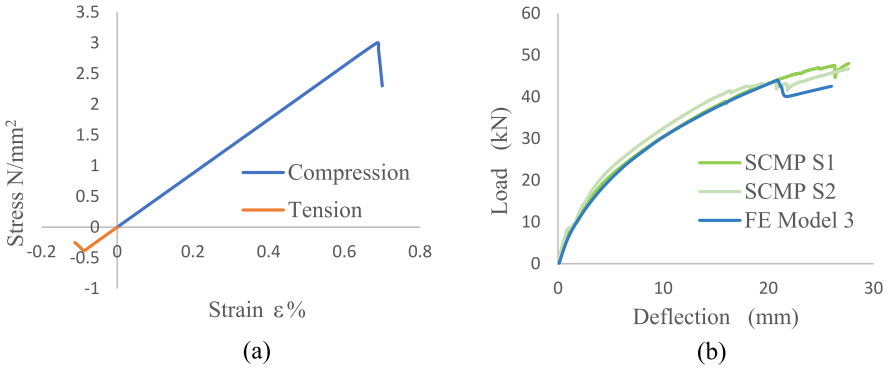

Fig. 21. (a) CDP model used in FEM 3; (b) Validation of FEM 3.

(Otoom et al., 2021). A displacement control simulation was carried out the same as the previous model. Both experimental and FEM load deflection curves were plotted in Fig. 21(b). Damaged layers were also examined in a similar manner to the first FEM.

4.2. Model verification

The FE models were validated using numerical and experimental results. The load deflection curve of FE model 1 shows a perfect correlation with the experimental results in the linear elastic region (Fig. 20(a)). The sudden load drops in the experimental results indicated the pipe failure. The core closer to the pipe invert failed first due to the formation of angled transverse shear crack through the layer followed by delamination. Secondly the core near the crown failed following the same failure modes. The FE model also captured the same failure modes, and the load–deflection relationship was very close to the sample 1 experimental results.

The Hashin damage results also showed a good comparison between

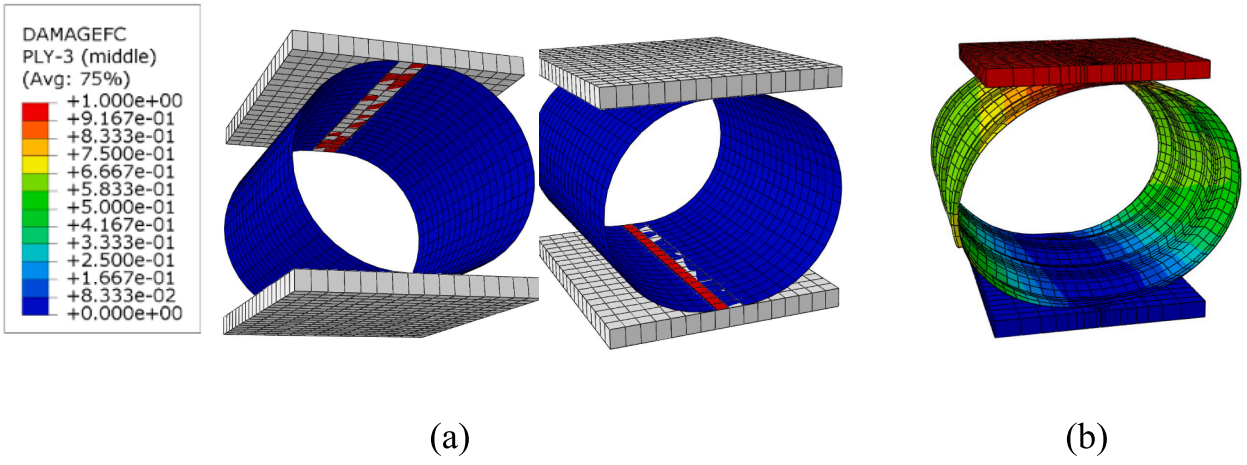

Fig. 22. (a) Hashin damage in the core- FEM 1; (b) Deformed CMP- FEM 2.

experimental observations (Fig. 22(a)). The red mesh indicates the damaged shell elements. The load–deflection curve of PPLT conducted for CMP alone is non-linear from the origin even though the curvature is non-prominent at the start. As depicted in Fig. 20(b), the FE model 2 results revealed a closely matching curve with the experimental results. The FE model 2 deformation due to the loadings was similar to the deformed shape of the CMP after the parallel plate load test (Fig. 22(b)).

Fig. 21(b) is a comparison of the parallel plate load test conducted for the sliplined corrugated metal pipe and the FE Model 3 results. A close agreement between the experimental and numerical results up to the 1st failure of FRP pipe was observed even though minor drops were not captured. The FE model also captured the non-linear load–deflection relationship of the sliplined pipe system. The failure loads of pipe samples 1 and 2 are 47.5 kN and 43.1 kN, respectively, whereas the failure load of the FE model was recorded as 44.0 kN. On the other hand, the predicted failure load from the FEM is reasonably close to sample 2. The load drop after failure seems comparatively higher. This may be due to the assumed fracture energies being slightly higher. The vertical deformations of samples 1 and 2 in relation to the failure load were 26.3 mm and 21.8 mm, respectively, while the FEM model failed when the deflection reached 20.9 mm. The sudden load drops in the experimental results indicated the FRP pipe core failures. The failure location is shown in Fig. 16(b). FE Model 3 pipe also failed at the same location as the load test.

The Hashin damage results of the FRP pipe of FE model 3 are shown in Fig. 23. Both compressive fibre damage (DAMAGEFC) and shear damage mechanisms (DAMAGESHR) of Abaqus FEM were triggered at the failure load. Red shell elements indicate that the core compressive stress and the shear stress have exceeded 8 MPa and 3.5 MPa respectively, satisfying the Hashin damage criteria mentioned above (Fig. 23).

5. Discussion

FRP pipes have been used in retrofitting corrugated metal pipes in many parts of the world (Department of Transport and Main Roads QLD, 2015; Ehsani 2019; Highways England, 2020). Parallel plate load test was the commonly used experiment to determine the structural performance of the FRP pipes. Most of the studies on FRP pipes as structural linings, only FRP pipes were tested neglecting any effects due to the corrugated metal pipe and the grout filled in the annular space of the sliplined pipe. This study was mainly focussed on the structural performance of the sliplined pipe system and any negative or positive effects due to the host pipe and the grout was investigated.

5.1. Pipe stiffness of sliplined pipe system

Pipe Stiffness (PS) is one of the most important parameters of the buried flexible pipe design which is used to assess the overall performance of the buried pipe system in presence of surrounding soil. Pipe stiffness for any given deflection is defined as $F/\Delta Y$ where F is the load in kN/m and ΔY is the vertical deflection in m (ASTM International, 2021). 3 % and 5 % vertical diameter change of the FRP pipe was selected for PS comparison (Fig. 24). Even though pipe stiffness is mainly used in flexible pipe design it was used in this study to compare the load carrying capacities of pipes before and after sliplining since SCMP exhibited some flexibility in comparison with rigid pipes. The average PS of CMP and FRP pips when deflection reached 3 % vertical diameter change was 1168 kPa and 3896 kPa, respectively. The average pipe stiffness of a sliplined pipe system was 12623 kPa. Due to the sliplining, load-carrying capacity was increased by 981 %. The average PS of CMP and FRP pips for 5 % deflection was 1077 kPa and 3319 kPa, respectively. The average pipe stiffness of a sliplined pipe system for the same deflection was 9882 kPa which is an 818 % increase in the load-carrying capacity. These increased load carrying capacities can be considered as the upper limit of the pipe stiffnesses because these values can come down in real life due to the reduced stiffness of corrugated metal pipes due to the deterioration and the varying grout strength from 1 MPa to 3 MPa. Further investigation is to be done to quantify the effects from the remaining strengths of corrugated metal pipes as an extension to this study. In this study intact CMP and 3 MPa grout was used, and FEM was created and those will be used as control samples.

Vertical Arching Factor (VAF) is one of the benefits which can be used to reduce the design loads of buried flexible pipes. When pipe is not stiffer than the surrounding soil VAF is less than 1 due to the arching action of the soil (Dhar et al., 2002). This mechanism is also known as positive arching action (Kang et al., 2013). Pipe flexibilities of the sliplined pipe system was compared with another parallel plate load test results available in the literature as sliplined pipe system stiffness was significantly higher than the FRP pipe stiffness. The results of PPLT conducted on a rigid pipe and a flexible pipe was selected for the comparison. The pipe stiffness of 66 mm thick concrete pipe (internal and external diameters are 518 mm and 584 mm respectively) was 450 MPa (Kraus et al., 2014). However, this stiffness relates to the crack initiation of the pipe for 0.07 % diameter change. The pipe stiffness for 5 % deflection was not available as pipe cracked when the vertical deflection reached to 0.07 % of the mean diameter. The pipe stiffnesses for 5 % deflection of a concrete lined CMP were approximately 2 MPa and 3 MPa for 20 mm and 40 mm concrete linings respectively (Kang and Davidson, 2010). The pipe stiffness for 5 % deflection of a 9 mm thick, 300 mm diameter solid wall FRP pipe was 718 kPa (Park et al., 2014). The pipe stiffness of the FRP sandwich pipe used in the study was 3.3 MPa whereas the same calculated for the sliplined pipe system was 9.9 MPa (Fig. 24(b)). While the rigid pipe failed upon reaching a 0.07 % diameter change, the tested SCMP maintained its structural integrity even after a

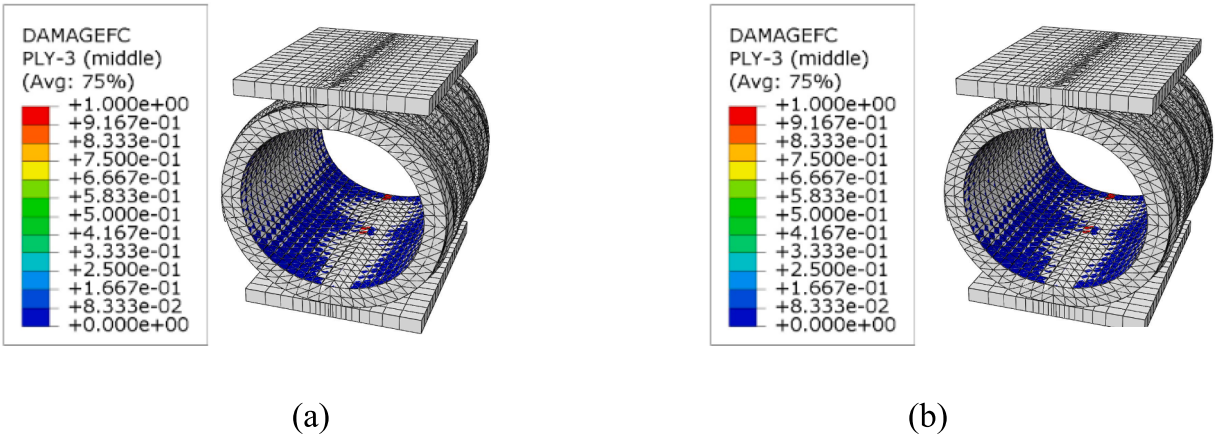

Fig. 23. (a) Hashin damage (Fibre Compression); (b) Hashin damage (Shear) FEM 3.

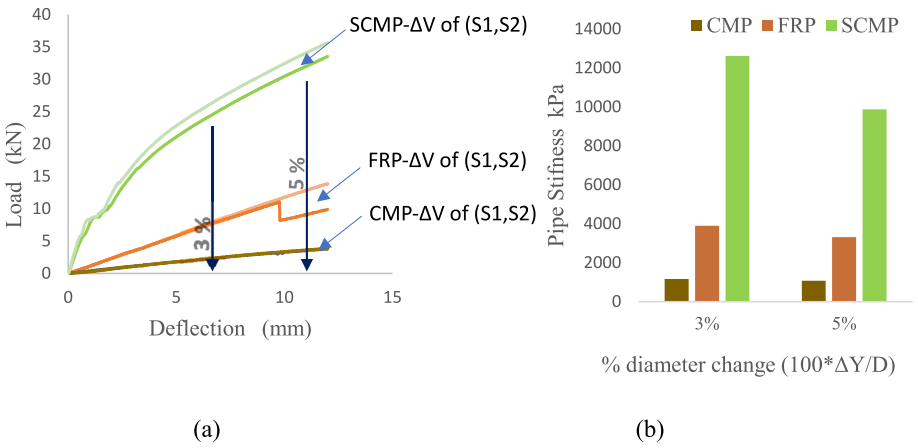

Fig. 24. (a) Load deflection curves; (b) Pipe stiffness comparison.

5 % diameter change. This demonstrates its notable flexibility, allowing it to withstand significant deformation without failure (Kraus et al., 2014).

5.2. Pipe deflection of sliplined pipe system

Deflection control is vital in berried culvert pipe design to assure the performance of supported road infrastructure. Therefore, many studies conducted focusing on pipe deflections (Masada 2000; Park et al., 2014). Both vertical and horizontal deflection of flexible pipe made of isotropic material can be calculated using elastic ring theory (Park et al., 2014). It can be proven that (ΔY/ΔX) ratio is 1.08 having divided the equation 1 by the equation 2 below (Park et al., 2014). Percentage ovality is another parameter which is used to quantify the geometric imperfection in pipe production (Sorour et al., 2019). Percentage pipe ovality can be used to compare the load deflection behaviour of pipe made of deferent material and defined in the Eq. (3) below. It can be observed that both pipe stiffness and stiffness of the surrounding soil have remarkable influence on (ΔY/ΔX) ratio based on the Spangler's experimental results (Masada 2000). When the surrounding soil was tamped, and stiff (ΔY/ΔX) ratio increased to a value as high as 1.31 whereas this ratio reduced to 0.94 for a CMP sample tested without compacting the surrounding soil (Masada 2000).Being a flexible pipe, FRP pipe tested in this study was also behaved in a similar manner. (ΔY/ΔX) ratio for PPLT conducted on FRP samples alone was 1.23 and it was increased to 1.37 when a same size FRP sample were tested as sliplined pipe system due to the external pressure from the grout (Fig. 25). The increase of (ΔY/ΔX) ratio implies the reduction of pipe ovality as shown in the Fig. 26. This reduction in ovality has benefits from both structural and hydraulic perspective.

$$\Delta Y = \frac{0.149PR^3}{EI} \tag{1}$$

$$\Delta X = \frac{0.137PR^3}{EI} \tag{2}$$

$$\%\,\text{Ovality} = \frac{100x(D_{max} - D_{min})}{D} \tag{3}$$

where E = modulus of elasticity, N/m^2, I = moment of inertia of wall cross section ($(1/12)*t^3$) per unit length of pipe, $m4/m = m^3$, R = mean radius of pipe, m, P = force, N/m run, ΔY = vertical deflection, m, ΔX = vertical deflection, m, D = original diameter, m, D_{max} = maximum diameter when deformed, m, D_{min} = minimum diameter when deformed, m.

The pipe deflection was calculated using the equation 1 using the load corresponding to the 3 % and 5 % diameter change. The total thickness of the pipe wall, 11.2 mm was considered in the moment of inertia calculation. The effective elastic modulus of the pipe wall along the circumferential direction determined by the material characterization were used. Effective elastic modulus of the pipe wall was 7087 MPa whereas corresponding loads were 7.8 kN and 13.15 kN for the FRP sample 1 (FRP S1) for the 3 % and 5 % vertical diameter change respectively. The calculated deflection using equation 1 and the experimental results were in good agreement (Table 5), indicating that equation 1 is usable to determine the deflection in the elastic region of FRP pipe with fewer input parameters, even though equations 1 and 2

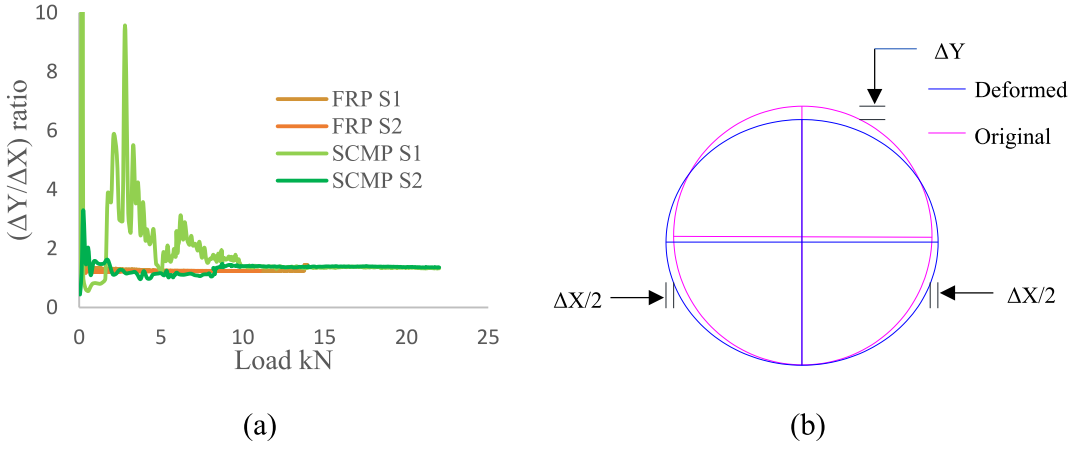

Fig. 25. (a) Variation of (ΔY/ΔX) ratio; (b) Illustration of pipe deformation measurement.

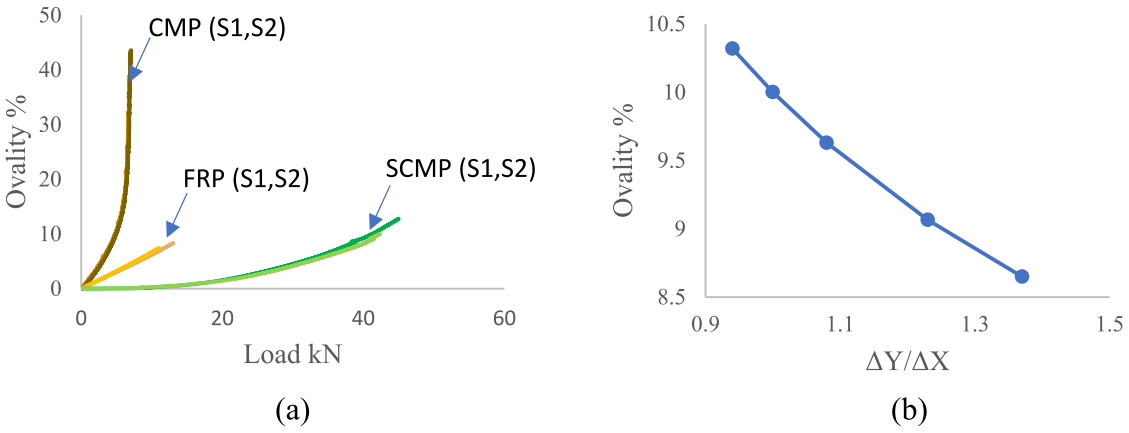

Fig. 26. (a) Variation of Ovality %; (b) Relationship between Ovality % and ΔY/ΔX.

Table 5
Comparison of experimental and numerical deflection results.

	Δ Experimental, mm	Δ Calculated, mm
3 % diameter change	6.8	7
5 % diameter change	11.3	11.3

were derived for pipe having isotropic materials. However, further investigations are required to investigate the limitations.

5.3. Failure mechanism of sliplined pipe system

Understanding the failure mechanisms of culvert pipes is crucial for both quality assurance testing after manufacturing and for conducting maintenance inspections. The invert was identified as the pipe failure location of the PPLT conducted on FRP pipe alone (Fig. 13(a)). This occurred due to the compressive failure of core. However, pipe could resist load until the springline failure of CFRP structural layer (Fig. 11). This is an added advantage of FRP sliplining method as it prevents possibilities of collapse in an event of unexpected load. According to the PPLT experimental observations the sliplined pipe system failed due to the core failure of the host pipe. The failure of the FRP pipe of sliplined pipe system occurred at the same location as the previous PPLT conducted for the FRP pipe alone. The main purpose of the core or honeycomb layer of a sandwich pipe is to increase the bending stiffness of the pipe wall. The above observations shows that the compressive strength of the core is the decisive factor for the pipe failure even though the core is not considered as a main structural layer.

The failure loads and deflection of the sliplined pipe were distinctly different from those of the FRP pipe itself (Fig. 16 (a)). The sliplined pipe system could resist more loads than the FRP pipe itself and it could deflect more than FRP pipe itself before the core failure. Based on the above observations, it can be concluded that the CMP and the grout provide a positive contribution to the structural performance of the sliplined pipe system. However, the actual contribution of remaining strength of CMP may be less than these figures as intact CMP was used in this study. Therefore, further studies are required to quantify the contribution of the CMP and grout and will be investigated as an extension to this study. The purpose of using FE models is to eliminate the necessity of conducting a series of pipe tests for different diameters which is time consuming and not economically viable. Since all the FE models were validated using the experimental results, these models will be used in parametric study of the ongoing study. On the other hand, unlike simple cylindrical pipe, the CMP or sliplined pipe system deflection calculation is not practicable without using FE analysis software due to the complex shape of the CMP and the non-linear behaviour of the grout CMP and the CLSM grout.

6. Conclusions

Structural performance of the FRP sliplining method was studied in this research. The load deflection behaviour of a FRP pipe as an individual pipe and as a host pipe of CMP sliplined pipe system was examined. Based on the experiments and the FE simulations following conclusions can be drawn.

1. The core failure of the FRP pipe governs the failure of the sliplined CMP system because of the lower mechanical properties core compared to the skin materials. The failure occurred at the invert when pipe was tested alone and as a host pipe in the sliplined system.
2. FRP sandwich pipe can resist the load even after the core failure until two inner structural layers reach their breaking stresses. After the core failures, three structural layers resist the external loads with a negligible contribution of the core until springline failure. Even though pipe serviceability deflection limit exceeds after first failure, pipe's ability of withstanding the external loads until structural layers are yielded by springline failure is an added advantage as far as road safety is concerned.
3. The load carrying capacity of deteriorated CMP can be improved by the FRP sliplining method. The host pipe and grout also contribute to resist external loads in addition to the new carrier pipe in the sliplined pipe system. Since an intact CMP pipe was used in the experiment, further experiments with deteriorated corrugated CMP are required to quantify actual increase in pipe load carrying capacity.
4. The surrounding grout improved the capacity and reduced the ovality of the FRP carrier pipe. This is due to the external pressure from the surrounding grout which reduces the horizontal diameter change.
5. The developed 3D finite element models considering accurate constituent material properties, geometric nonlinearity and behaviour of grout and steel can adequately predict the load–deflection response of the sliplined CMP using FRP sandwich pipe until the sliplined pipe system failure. The FEM predicted failure modes are in good correlation with those observed in experiments.

The above findings provide a better understanding of the behaviour of the sliplined corrugated metal pipe system. These findings, experimental data and FEM analysis could be useful for practising engineers in designing CMP strengthening systems using FRP sandwich pipes. Additionally, the mechanical properties will be used to design a more economical culvert pipe. This will be implemented by conducting a parametric study to determine if the remaining strength of CMP can be incorporated in sliplined pipe system as an extension to this study. Further development is, however, recommended to quantify the

influence of the remaining strength of the deteriorated CMP and CLSM grout.

7. Research data

The raw/processed data required to reproduce these findings cannot be shared at this time as the data also forms part of an ongoing study.

CRediT authorship contribution statement

Aluth Premasuriya: Writing – original draft, Visualization, Validation, Methodology, Investigation, Formal analysis, Data curation, Conceptualization. **Weena Lokuge:** Writing – review & editing, Validation, Supervision, Resources, Project administration, Methodology. **Warna Karunasena:** Writing – review & editing, Validation, Supervision, Methodology. **Allan C. Manalo:** Writing – review & editing, Supervision, Methodology.

Declaration of competing interest

The authors declare that they have no known competing financial interests or personal relationships that could have appeared to influence the work reported in this paper.

Acknowledgments

The first author acknowledges the support received through the Australian Government research training program (RTP) fees offset place scholarship. The authors would like to acknowledge the support of QuakeWrap Pty. Ltd., Australia (owned by Hychem), for the materials supply, casting of samples and providing technical support and Holcim Australia for the flowable mortar mix supply. Also, sincere thanks for the technical staff at the Centre for Future Material (CFM), University of Southern Queensland, Toowoomba for their assistance in conducting the experimental work of this study.

Data availability

Data will be made available on request.

References

Abdellatef, M., Chennareddy, R., Taha, M.M.R., 2021. Design of GFRP Slip Liner for Retrofitting Corroded Metal Culverts Tran-SET 2021.
Al-saadi, A.U., Aravinthan, T., Lokuge, W., 2019. Effects of fibre orientation and layup on the mechanical properties of the pultruded glass fibre reinforced polymer tubes. Engineering Structures 198.
ASTM International, 2016a. Standard Test Method for Compressive Properties of Polymer Matrix Composite Materials Using a Combined Loading Compression (CLC) Test Fixture. ASTM International, Pennsylvania.
ASTM International, 2016b. Standard Test Method for Preparation and Testing of Controlled Low Strength Material (CLSM) Test Cylinders. ASTM International, Pennsylvania.
ASTM International, 2017. Standard Test Method for Splitting Tensile Strength of Cylindrical Concrete Specimens. ASTM International, Pennsylvania.
ASTM International, 2019. Standard Test Method for Shear Properties of Composite Materials by the V-Notched Beam Method. ASTM International, Pennsylvania.
ASTM International, 2021. Determination of External Loading Characteristics of Plastic Pipe by Parallel-Plate Loading. ASTM International, Pennsylvania.
Dassauts Systems, 2019. Abaqus CAE, V2019 ed.
Department of Transport and Main Roads QLD, 2015. Criteria for Inspection, Life Extension and Rehabilitation of Circular Corrugated Metal Culverts.
Dhar, A.S., Moore, I.D., McGrath, T.J., 2002. Evaluation of Simplified Design Methods for Buried Thermoplastic Pipe, Pipeline Division Specialty Conference, Cleveland, Ohio, United States.
Ehsani, M., 2019. A new FRP solution for reconstruction of deteriorated pipes and culverts, International No-Dig 2019 37th International Conference and Exhibition. Florence, Italy.
El-Taher, M., Moore, I.D., 2008. Finite Element Study of Stability of Corroded Metal Culverts. Transportation Research Record: Journal of the Transportation Research Board 2050, 157–166.
García, D.B., Moore, I.D., 2015. Performance of deteriorated corrugated steel culverts rehabilitated with sprayed-on cementitious liners subjected to surface loads. Tunnelling and Underground Space Technology 47, 222–232.
Garifullin, M., Mela, K., Renaux, T., Izabel, D., Holz, R., Fauth, C., 2021. Load-bearing capacity of cold-formed sinusoidal steel sheets. Thin-Walled Structures 161.
Gonilha, J.A., Correia, J.R., Santos, M.S., Ferreira, J.G., Branco, F.A., Gomes, R.C., 2022. GFRP Composite Culverts for Hydraulic and Agricultural Underpasses: Structural Behavior, Design, and Application. Journal of Composites for Construction 26.
Gordon, R., Boully, G., 1998. Bridges - Planning for the future. International symposium of heavy vehicle weights and dimensions, Maroochydore, Australia.
Hafezolghorani, M., Hejazi, F., Vaghei, R., Jaafar, M.S.B., Karimzade, K., 2018. Simplified Damage Plasticity Model for Concrete. Structural Engineering International 27, 68–78.
Hashin, Z., 1980. Failure Criteria for Unidirectional Fiber Composites. Journal of Applied Mechanics 47, 329–334.
Heywood, R., Ellis, T., 1998. Australias-new-bridge-design-load-improving-transport-productivity. International symposium of heavy vehicle weights and dimensions, Maroochydore, Australia.
Heywood, R., Pritchard, R., 2011. The Rehabilitation of Corrugated Metal Culverts 8th Austroads Bridge Conference Sydney. New South Wales, Australia.
Highways England, 2020. Management of corrugated steel buried structures.
Hudson, J.A., Cardenas, H., Matthews, J., Alam, S., 2023. Performance evaluation of deteriorated and rehabilitated corrugated metal pipe culverts using multiphysics simulation. Tunnelling and Underground Space Technology 131.
International Organization for Standardization, 2021. Determination of tensile properties-Test conditions for isotropic and orthotropic fibre-reinforced plastic composites. International Organization for Standardization, Geneva.
Kanagaraj, A.S., 2020. Behavior of solid wall and sandwich fiber reinforced polymer liners used for rehabilitation of buried pipes. Dalhousie University, Nova Scotia, Canada, Faculty of Graduate Studies.
Kang, J.S., Davidson, J.S., 2010. Structural effects of concrete lining for concrete-lined corrugated steel pipes. Structure and Infrastructure Engineering 1–11.
Kang, J.S., Stuart, S.J., Davidson, J.S., 2013. Analytical evaluation of maximum cover limits for thermoplastic pipes used in highway construction. Structure and Infrastructure Engineering 9, 667–674.
Kraus, E., Oh, J., Fernando, E.G., 2014. Impact of Repeat Overweight Truck Traffic on Buried Utility Facilities. Journal of Performance of Constructed Facilities 28.
Kunecki, B., Janusz, L., Korusiewicz, L., 2016. Load Tests of Deteriorated Steel Pipe, the Sixth International Conference on Structural Engineering, Mechanics and Computation.
Lantorcomposites.com, 2021.
Masada, T., 2000. Modified Iowa Formula for Vertical Deflection of Buried Flexible Pipe. J Ournal of Transpotation Engineering 126, 440–446.
Minnesota Department of Transport, 2016. Large Corrugated Metal Pipe Repair Techniques: A Survey of Practice and Related Resources.Osborn, L., 2009. Trenchless renewal of culverts and storm sewers. American Society of Civil Engineers.
Otoom, O.F., Lokuge, W., Karunasena, W., Manalo, A.C., Ozbakkaloglu, T., Ehsani, M.R., 2022. Flexural behaviour of circular reinforced concrete columns strengthened by glass fibre reinforced polymer wrapping system. Structures 38, 1326–1348.
Otoom, O.F., Lokuge, W., Karunasena, W., Manalo, A.C., Ozbakkaloglu, T., Thambiratnam, D., 2021. Experimental and numerical evaluation of the compression behaviour of GFRP-wrapped infill materials. Case Studies in Construction Materials 15.
Park, J.S., Hong, W.H., Lee, W., Park, J.H., Yoon, S.J., 2014. Pipe Stiffness Prediction of Buried GFRP Flexible Pipe. Polymers & Polymer Composites 22 (1), 17–24.
Prabhakar, M., Rajini, N., Ayrilmis, N., Mayandi, K., Siengchin, S., Senthilkumar, K., Karthikeyan, S., Ismail, S.O., 2019. An overview of burst, buckling, durability and corrosion analysis of lightweight FRP composite pipes and their applicability. Composite Structures 230, 111419.
Rahmaninezhad, S.M., Han, J., Al-Naddaf, M., Jawad, S., Parsons, R.L., Liu, H., 2020. Field evaluation of performance of corroded corrugated steel pipe before and after sliplining rehabilitation. Tunnelling and Underground Space Technology 102, 103442.
Rahmaninezhad, S.M., Han, J., Al-Naddaf, M., Parsons, R.L., 2019. Behavior of Sliplined Corrugated Steel Pipes under Parallel-Plate Loading. Journal of Materials in Civil Engineering 31, 04019242.
Regier, C., Moore, I.D., Hoult, N.A., 2018. Remaining Strength of Deteriorated Corrugated Steel Culverts. Journal of Pipeline Systems Engineering and Practice 9.
Sorour, S.S., Shazly, M., Megahed, M.M., 2019. Limit load analysis of thin-walled as-fabricated pipe bends with low ovality under in-plane moment loading and internal pressure. Thin-Walled Structures 144.
Standards Australia, 1998. Burried Flexible Pipelines, AS/NZS 2566.1-1998 Standards Australia Sydney.
Standards Australia, 2011. Burried Corrugated Metal Structures, AS/NZS 2014.1-2011. Standards Australia, Sydney.
S. Australia Burried Flexible Pipelines 2022 Standards Australia Sydney.
Taha, M.M.R., Halter, S.B., 2019. Cost-Effective Methods to Retrofit Metal Culverts Using Composites. United States.
Tetreault, J., Moore, I.D., Hoult, N.A., 2020. Laboratory Study on Effect of Grout Choice on Culvert Rehabilitation Using Sliplining. Journal of Pipeline Systems Engineering and Practice 11.
Wong, K.J., Gong, X.J., Aivazzadeh, S., Tamin, M.N., 2011. Tensile behaviour of anti-symmetric CFRP composite. Procedia Engineering 10, 1865–1870.

Zhang, Y., Wong, R.-C.-K., 2023. Effect of corrosion on buried pipe responses under external load: Experimental and numerical study. Tunnelling and Underground Space Technology 132.
Zhao, J.Q., Daigle, L., Rajani, B.B., 2004. Effect of eccentricity and bonding on behaviour of sliplined pipe. Tunnelling and Underground Space Technology 19, 97–110.
Zhu, H., Wang, T., Wang, Y., Li, V.C., 2021. Trenchless rehabilitation for concrete pipelines of water infrastructure: A review from the structural perspective. Cement and Concrete Composites 123.